PHYSICAL REVIEW D VOLUME 43, NUMBER 4 15 FEBRUARY 1991

Primordial nucleosynthesis with horizon-scale curvature fluctuations

Hannu Kurki-Suonio
Department of Physics and Atmospheric Science, Drexel University, Philadelphia, Pennsylvania 19104 and Lawrence Livermore National Laboratory, University of California, Livermore, California 94550[*]

Joan Centrella
Department of Physics and Atmospheric Science, Drexel University, Philadelphia, Pennsylvania 19104

(Received 2 July 1990)

We have used a plane-symmetric numerical relativity and hydrodynamics code to study the effect of horizon-scale inhomogeneities in the energy density and spacetime curvature on primordial nucleosynthesis. ^{2}H, ^{3}He, and ^{7}Li yields are chiefly determined by the local baryon-to-photon ratios during nucleosynthesis, whereas ^{4}He depends on previous dynamical history which determines how many neutrons survive until nucleosynthesis. Strong $(\delta\rho/\rho\sim 1)$ inhomogeneities are allowed by the observed abundances. Inhomogeneities usually raise both ^{4}He and ^{2}H but in some cases a nonadiabatic curvature inhomogeneity leads to a ^{4}He yield below the standard-model result with the same average baryon-to-photon ratio.

I. INTRODUCTION

The standard homogeneous big-bang nucleosynthesis model has been remarkably successful[1-3] and forms a cornerstone of the big-bang theory itself. Does this good agreement with observations indicate that the early Universe was homogeneous indeed? The other evidence of homogeneity we have, that from the isotropy of cosmic-microwave-background radiation, refers to a much later era, 10^5 yr from the singularity, whereas nucleosynthesis took place during the first minutes of the Universe.

The observational data on the primordial abundances of light elements is summarized by Boesgaard and Steigman.[2] They give the value 0.239±0.015 for the primordial ^{4}He abundance and 1.6–20×10^{-5} for the ^{2}H/H ratio. They also give an upper limit $(^2\mathrm{H}+{}^3\mathrm{He})/\mathrm{H} < 6-10\times10^{-5}$. (In this paper ^{2}H, ^{3}He, ^{4}He, ^{7}Li denote mass fractions, whereas ^{2}H/H, ^{3}He/H, ^{4}He/H, ^{7}Li/H are number ratios.) We adopt here $^2\mathrm{H}=1.5\times10^{-4}$ $(^2\mathrm{H}/\mathrm{H} =10\times10^{-5})$ as the upper limit, which is an order of magnitude higher than the present interstellar value $^2\mathrm{H}=2.0\times10^{-5}$. This difference can be explained by depletion of deuterium in stars during galactic evolution, with the expectation that a large part of this processed deuterium will show up as interstellar ^{3}He. Finally, there are two "primordial" values for ^{7}Li. Observations of Population II stars give a low value $^7\mathrm{Li}/\mathrm{H}=0.7-1.8\times10^{-10}$, yielding $^7\mathrm{Li}=3.7-9.5\times10^{-10}$. Population I stars give a higher value $^7\mathrm{Li}/\mathrm{H}=0.4-1.6\times10^{-9}$, or $^7\mathrm{Li}=2.1-8.4\times10^{-9}$.

To fit the standard homogeneous and isotropic cosmological model with nucleosynthesis to the observed primordial abundances one adjusts the sole parameter, the baryon-to-photon ratio $\eta=n_b/n_\gamma$. Using the newest reaction rates,[4,5] a yield of $^4\mathrm{He}=0.239$ is obtained in the standard model with $\eta=2.2\times10^{-10}$. This gives an abundance $^2\mathrm{H}=1.9\times10^{-4}$, or a number ratio $^2\mathrm{H}/\mathrm{H}=1.2\times10^{-4}$, larger than the present interstellar value (see above). On the other hand, a low value of $^2\mathrm{H}/\mathrm{H}=6\times10^{-5}$, or $^2\mathrm{H}=9\times10^{-5}$, is obtained with $\eta=3.5\times10^{-10}$; this raises the ^{4}He to 0.244. The present interstellar value for ^{2}H corresponds to $\eta=9\times10^{-10}$ and $^4\mathrm{He}=0.252$, which is somewhat high,[6] but probably acceptable. Thus, although the fit is good, we are still forced to choose between a high value of ^{2}H or a high value of ^{4}He, or to compromise by having somewhat high primordial values for both. The compromise position may be eliminated and the choice made for us if the question of primordial ^{7}Li is clarified. The Population II observations correspond to $\eta=1.5-4\times10^{-10}$, while Population I data correspond to $\eta=5.3-11\times10^{-10}$. (The other two ranges giving Population I abundances of ^{7}Li, $\eta=0.07-0.11\times10^{-10}$ and $\eta=0.6-1.2\times10^{-10}$ are ruled out by deuterium overproduction.) The above kind of detailed analysis[3] can be altered by inhomogeneities and this is the second motivation in studying inhomogeneous nucleosynthesis.

Effects of inhomogeneity on nucleosynthesis have been studied before.[7-14] There are two basic types of inhomogeneity to consider.[15] In isocurvature fluctuations[1] the baryon-number density is inhomogeneous but the energy density of the Universe is homogeneous. These are thus fluctuations in the baryon-to-photon ratio n_b/n_γ (or in entropy/baryon) (we reserve the notation η for the average, or total, value of this ratio). Since the baryons are a "test fluid," in this case spacetime is spatially homogeneous, and general relativity is not involved except for the universal expansion. The n_b/n_γ inhomogeneity evolves through diffusion only. For the distance scales we are interested in here diffusion is insignificant; thus the n_b/n_γ inhomogeneity remains constant in amplitude and in comoving distance scale.

Adiabatic curvature fluctuations refer to energy-density inhomogeneity with n_b/n_γ homogeneous. Since energy density is a source of spacetime curvature this is a more difficult case to study unless the distance scale λ of the inhomogeneity is sufficiently different from the horizon scale L_H. For $\lambda \gg L_H$ the regions of different energy densities can be considered as independent homogeneous universes. Since homogeneous nucleosynthesis depends only on n_b/n_γ, this does not produce significant differences from the standard model.[9] If $\lambda \ll L_H$ the spacetime sees just the average density and we get an essentially homogeneous expansion. The most involved case $\lambda \sim L_H$ can be treated perturbatively if the amplitude is small but for stronger inhomogeneity one has to resort to numerical relativity.

The possible initial energy-density fluctuations do not exhaust all possible (adiabatic) curvature fluctuations. Even with a constant initial density we can introduce inhomogeneity in the expansion rates along different directions. These additional degrees of freedom represent gravitational waves. In our case they are long (horizon-scale) wavelength, and appear as oscillating anisotropy in the universal expansion.

Since isocurvature fluctuations do not require numerical relativity, in this paper we study curvature fluctuations only. In addition to studying adiabatic curvature fluctuations, we combine them with n_b/n_γ inhomogeneity for nonadiabatic curvature fluctuations.

Numerical relativity was first applied to nucleosynthesis with strong horizon-scale curvature inhomogeneities by Centrella, Matzner, Rothman, and Wilson[16] (CMRW). This study was limited by the supercomputer time available then. With better supercomputer access we have now done a more extensive study with improved diagnostics and higher resolution. We have also updated the nuclear reaction rates and extended the reaction network to include ^{7}Li.

II. ABOUT THE CODE

In our investigation we have employed an inhomogeneous nucleosynthesis code which is a hybrid of two codes developed separately. The spacetime and hydrodynamical evolution is provided by the plane-symmetric cosmology code of Centrella and Wilson.[17,18] The isotope abundance evolution is computed with the nucleosynthesis code developed by Rothman, Matzner, and Kurki-Suonio.[19,20] These codes were combined by CMRW. Since then the cosmology part of the code has remained essentially the same, except that we now store several additional quantities to assist in viewing the simulation. The nucleosynthesis connection poses its own requirements for setting the initial data, and we have developed this procedure further, as outlined below. The nucleosynthesis part has been updated to include the newest reaction rates and the network has been enlarged and includes now all cosmologically significant isotopes up to $A=7$.

The code spacetime is plane symmetric with periodic boundary conditions; i.e., we use a Cartesian xyz-coordinate system with the inhomogeneity in the z direction only. Thus the code is a one-dimensional (1D) code in the sense of functions varying only in one spatial dimension plus time; the spacetime itself is fully 4D. A 1D code is the only practical possibility for nucleosynthesis, because of the lengthy nuclear reaction calculations to be performed in each computational zone. And plane symmetry is quite appropriate for our case, since we are not dealing with a single collapsed object, but rather with a representative piece of the Universe at an era before matter clumped into galaxies. We are studying the effects of inhomogeneities on primordial nucleosynthesis without any model to specify the shapes of these inhomogeneities. Of the 1D symmetries, plane symmetry is the only one that respects the Copernican principle by having no preferred positions on the grid.

Our aim is not so much to determine definite isotope yields for specific inhomogeneity parameter values, but rather to find out the type and strength of the effects we can typically expect and the mechanisms through which they come about. Effects present in plane-symmetric models will play a role with more general inhomogeneities also, although there may be some additional effects peculiar to other geometries that we cannot discover here.

The gauge freedom in general relativity allows us to arbitrarily choose the slicing of the spacetime into three-dimensional slices and the evolution of the xyz coordinates from one slice to the next. These choices are represented by the lapse function α and the shift vector β^i, respectively. We use constant mean curvature slicing, so that α is found from the evolution equation for tr$K$ (trace of extrinsic curvature of the slice) with the requirement that tr$K$=tr$K(t)$ only. The shift vector is chosen so that the three-metric of each slice remains diagonal

$$\gamma=\mathrm{diag}(A^2, A^2h^2, A^2) .$$

A difficulty in numerical relativity is that data on each slice have to satisfy constraint equations. This interferes with our ability to set initial data as we choose. The intrinsic and extrinsic curvature of a slice can be separated (in various ways) into dependent and dependent variables. Once the independent variables are known, the dependent variables are determined from the constraint equations. We have chosen the dependent variables to be $h(z)$, to be found from the Hamiltonian constraint, and $K^z_z(z)$, to be found from the momentum constraint. This differs from the usual York[21] prescription.

We set the initial slice by first choosing the (inhomogeneous) radiation density and flow velocity, baryon density, and the freely specifiable extrinsic curvature component $K_1(z) \equiv K^x_x - K^y_y$. tr$K$ is then set to the value that a homogeneous Bianchi type-I universe would have for the same average energy density. We set $A(z)\equiv 1$ for the initial slice, where A^2 is the conformal factor, and then solve the constraint equations. Since the volume of each zone is multiplied by $h(z)$, this modifies our original radiation and baryon distributions.

Once the constraints are satisfied on the initial slice, the evolution equations preserve them for all subsequent slices. In a numerical calculation the data may however gradually drift and begin to violate the constraints. For better stability, our code is fully constrained; i.e., the constraint equations are explicitly solved on each slice.

The relativistic hydrodynamic equations are treated in the code by the Wilson[22] method, where the equations are written to resemble Newtonian equations as much as possible. Strong initial inhomogeneities develop into shocks. We use artificial viscosity to spread the shock front over several zones.

For a more detailed description of the cosmology code, see Refs. 17 and 18.

Connecting the nucleosynthesis and cosmology codes is simplified by the fact that the influence is in one direction only. The baryons make a negligible contribution to the total energy density during the nucleosynthesis epoch and thus do not affect the hydro- and geometrodynamics. Thus the cosmology part runs essentially independently, providing thermodynamical information which is then used to calculate the nucleosynthesis in each zone. The primordial radiation and/or plasma is treated as a perfect fluid. The equation of state, relating pressure, temperature, and energy density of a zone is the one used in primordial nucleosynthesis calculations. It is close to $p=\frac{1}{3}\rho$, but deviates somewhat from this during electron-positron annihilation, because electrons become nonrelativistic. Temperature, of course, does not appear in the dynamical equations, and is only needed for nucleosynthesis. We assume three flavors of massless neutrinos.

The baryons are assumed to follow the hydrodynamical flow. That is, the code (as used in this investigation) does not allow for diffusion of nucleons. The possibility that the cosmological quark-hadron phase transition could have generated inhomogeneity in the baryon density affecting nucleosynthesis significantly has received a great deal of attention recently.[23-32] In this scenario diffusion is of crucial importance, because of the expected small distance scale of the inhomogeneity. We have studied this topic recently, first by modifying the code described here to include diffusion,[33] and then with a homogeneous background spacetime code written specifically for the purpose.[34-36] This is however a separate line of inquiry that does not overlap with the present investigation, because the distance scales of interest are so very different. At the nucleosynthesis epoch diffusion is important in distance scales of kilometers (corresponding to present light hours). This is many orders of magnitude smaller than the horizon scale at that time, which is measured in light seconds (hundreds of present light years). Here we are interested in inhomogeneities with distance scales comparable to the horizon, where general relativistic effects become important.

Our nuclear reaction network includes the nine $A \leq 7$ isotopes n, p, ^{2}H, ^{3}H, ^{3}He, ^{4}He, ^{6}Li, ^{7}Li, and ^{7}Be, whose abundances we calculate. The gap at $A=8$ (no isotopes with lifetimes longer than about one second) provides a natural cutoff. This is the minimum network that allows us to calculate the cosmologically significant isotopes p, ^{2}H, ^{3}He, ^{4}He, and ^{7}Li (n, ^{3}H, and ^{7}Be are unstable with half-lives of 10.35 min, 12.3 yr, and 53 days, respectively), except that ^{6}Li, which is produced in insignificant quantities could probably be dropped without affecting the results noticeably.

Because the nuclear reactions have to be calculated in each zone, an inhomogeneous nucleosynthesis code becomes very time consuming. The computer time required grows at least as the square (cube, without vectorizing) of the number of isotopes. Indeed, the nucleosynthesis part completely dominates the time consumption of the code. To be able to do a large number of runs it was crucial to keep the number of isotopes at minimum. To ascertain that the omission of heavier isotopes did not affect the results, especially the yield of $A=7$ isotopes, we included in the reaction network the reactions leading to the heavier isotopes as sinks, and studied the effect of turning these sinks on and off (a full larger network would give a result in between). The importance of these heavier isotopes increases with increasing baryon/photon ratio. We found that they can be ignored for $n_b/n_\gamma < 10^{-8}$. For larger baryon densities the yield of ^{7}Li may be reduced by reactions leading to heavier isotopes. A homogeneous $\eta=10^{-7}$ model produces lg $^7\mathrm{Li}=-6.6$ with sinks turned off and lg $^7\mathrm{Li}=-6.7$ with sinks turned on. (We give all isotope abundance results as mass fractions.)

We use the reaction rates from the 1988 compilation by Caughlan and Fowler.[4] We include all 39 strong reactions involving nuclei with $A \leq 7$ (except ^{6}He) from this compilation, although about half of them could be ignored without changing the results. Rates for (n,γ) reactions and $^7\mathrm{Be}(n,\alpha)^4\mathrm{He}$ not included in this compilation are those used by Schramm and Wagoner,[37] except that the newer estimate for $^7\mathrm{Li}(n,\gamma)^8\mathrm{Li}$ by Malaney and Fowler[38] is used. Altogether our network has 45 strong reactions, with 33 reverse reactions (12 reactions leading to $A>7$ are treated as sinks with reverse reactions ignored).

Notable revisions in these reaction rates from the previous, 1985,[39] compilation are $^2\mathrm{H}(d,n)^3\mathrm{He}$, $^2\mathrm{H}(d,p)^3\mathrm{H}$, $^3\mathrm{He}(d,p)^4\mathrm{He}$, $^4\mathrm{He}(t,\gamma)^7\mathrm{Li}$, and $^7\mathrm{Be}(n,p)^7\mathrm{Li}$. The effect of these is to raise the ^{7}Li yields by 20–50 % and the ^{4}He yields by 0.0006–0.0008.

We use $\tau_n=896s$ for the neutron mean lifetime[5] (half-life of 10.35 min). The weak $n \leftrightarrow p$ rates are obtained by numerical integration, and multiplied[8] with a Coulomb correction factor 0.98. Additional small corrections calculated by Dicus *et al.*[40] are represented by subtracting 0.001 from all ^{4}He mass fractions. We mention these details because they are necessary for accurate comparison with other work. We checked the accuracy of our reaction network by doing a sequence of homogeneous runs (with different values of η) and comparing with the results of Yang *et al.*[1] (YTSSO). To do this we temporarily replaced the rates of 7 important reactions with older rates used in YTSSO, and the numerical integration of $n \leftrightarrow p$ rates with the Wagoner[8] polynomial, and applied a -0.003 ^{4}He correction to mimic YTSSO. The results for ^{2}H and ^{3}He agreed within 3%, for ^{7}Li within 6%, and for ^{4}He within 0.001, which is quite satisfactory in this context. With the present network our ^{4}He yield is somewhat higher, for two reasons. (1) The new rates raise it by 0.0006–0.0008. (2) Instead of a -0.003 correction we use numerical integration of $n \leftrightarrow p$ rates (this was the largest component of this correction; its effect in our results is -0.0011–-0.0013), and apply a remaining correction -0.001 (this does not quite add up to -0.003, but agrees with Dicus *et al.*[40]). Thus we now get ^{4}He about 0.002 higher than YTSSO for the same τ_n. With the new rates ^{7}Li is significantly higher, whereas the changes in ^{2}H and ^{3}He are not significant, except that ^{2}H is lower for large η.

The neutron/proton ratio begins to deviate significantly from equilibrium at around $T_9 \sim 20$ ($T_9 \equiv T/10^9$ K). A nucleosynthesis run should thus be started above that temperature. For numerical reasons and to have better control over the inhomogeneity close to the main nucleosynthesis action ($T_9 = 0.5-1$) the cosmology is initialized at a lower temperature, for most runs about $T_9 \sim 10$, $t \sim 1$ s. The code, without the nucleosynthesis part, is then run backward in time to $T_9 \sim 20$, $t \sim 0.1$ s, where the nucleosynthesis is initialized, and then the code is run forward, with nucleosynthesis, to $T_9 \sim 0.1$, $t \sim 10\,000$ s, at which time the primordial abundances have been determined. Since the baryon density is dynamically insignificant, we reset it to a desired profile at nucleosynthesis initialization, taking care that the initial data has the required average n_b/n_γ. In some cases we wanted better control of the baryon density during the main nucleosynthesis action. We achieved this with a more complicated scheme: after initializing the cosmology we ran it forward, initialized the baryon density at a later time, then ran it backward, initialized the nucleosynthesis at an earlier time, and then finally ran the full code forward to obtain the evolution.

In most of our runs the length of our computational grid, representing one period in the z direction, was set to two horizon radii, or 4.3 light seconds, at initialization. Because of better availability of supercomputer time, we were able to use a finer grid than in CMRW, where 50 zones were used. Based on comparing runs using 50, 100, and 150 zones (Table I) we deemed acceptable the accuracy achieved with 100 zones. These runs were the same as our inhomogeneous run 4 (see below), except that the comparison was run when we still had the older, 1985, reaction rates. The homogeneous run is given for comparison, since the effect we are studying is the change from this due to the inhomogeneities. Thus, according to the 150-zone run the effect on ^{4}He is to reduce it by 0.0053, and the 100-zone run is within 4% of this, 0.0051. However the 50-zone run does not see this effect, and instead reports a slight increase. To use 200 or 300 zones in this investigation would not have been possible because of computer time cost.

III. RESULTS

In our inhomogeneous initial data we have the freedom to set the energy density E, the z-momentum density S_z, the baryon density D, and the extrinsic curvature variable K_1. As a reference point we use a homogeneous run with a baryon/photon ratio $\eta = 10^{-9.5}$. This run produced the mass fractions (^{4}He, ^{2}H, ^{3}He, ^{7}Li) = (0.2428, 1.04×10^{-4}, 3.46×10^{-5}, 6.77×10^{-10}). Keeping the average n_b/n_γ the same we introduced various inhomogeneities.

In run 1 we studied the effect of inhomogeneity in energy density. On the initial slice the energy density was set with an inhomogeneity of $\delta E/E \sim 1$. More precisely, we set

$$E = E_0\left[1+\sum_{n=1}^{5} E_n \cos(2n\pi z/L_{\text{grid}})\right],$$

with the relative amplitudes of the different modes $E_n = 0.6$, 0.3, 0.15, 0.075, 0.0375. The profile has a density peak at the edge of the grid. The average energy density E_0 was set to correspond to a radiation temperature $T_9 = 10$ and the grid length L_{grid} equal to two horizon lengths at this moment. We set $S_z = K_1 = 0$ initially. The code then solved the initial constraints modifying the E profile somewhat. Most significantly, solving the Hamiltonian constraint for the metric variable h gave a rather inhomogeneous h, making the zones different in volume, and thus altering the volume average of E from E_0. Defining

$$\delta E/E = \frac{E_{\max}-E_{\text{av}}}{E_{\text{av}}},$$

the inhomogeneous h changed the initial $\delta E/E$ from 1.16 to 1.04—because the low density zones got a smaller volume, raising E_{av}. The code then ran backward until $t \sim 0.2$ s, $T_9 \sim 20$ where the nucleosynthesis was initialized and then forward until $T_9 \sim 0.1$ with nucleosynthesis. The fluid remains fairly stationary in the grid until the inhomogeneity enters the horizon at $T_9 \sim 5$ ($t \sim 4$ s). The pressure difference then sets the fluid into motion and after these waves cross they develop into shocks that move across the grid many times, gradually weakening. The nucleosynthesis in this run had a fairly homogeneous production of the trace isotopes ^{2}H, ^{3}He, and ^{7}Li. This could have been expected from constant n_b/n_γ. There was some inhomogeneity in the ^{4}He production. See Table II. We defer a detailed discussion of the effects to run 3d, where they were similar, but more pronounced. The effects—deviations from homogeneous nucleosynthesis—are rather weak in run 1. This is because during nucleosynthesis most of the inhomogeneity is actually much smaller than the $\delta E/E \sim 1$ at the initial time.

We would like to see the effect of a stronger inhomo-

TABLE I. Effect of zone size (nonadiabatic $\eta = 10^{-9.5}$ run with 1985 rates).

	^{4}He	lg^{2}H	lg^{3}He	lg^{7}Li
Homog.	0.2419	-3.96	-4.45	-9.35
50 zones	0.2428	-3.87	-4.44	-9.15
100 zones	0.2377	-3.77	-4.45	-9.01
150 zones	0.2375	-3.76	-4.43	-8.97

TABLE II. The total (average) isotope yields (mass fractions) as well as the minimum and maximum local values in nine runs compared to the homogeneous standard-model result. All runs have $\eta=10^{-9.5}$.

Run No.	^{4}He	^{2}H	^{3}He	^{7}Li	^{4}He	^{2}H(10^{-4})	^{3}He (10^{-5})	^{7}Li (10^{-10})
Homog.	0.2428	1.04×10^{-4}	3.46×10^{-5}	6.77×10^{-10}	Min–Max	Min–Max	Min–Max	Min–Max
1	0.2464	1.11×10^{-4}	3.46×10^{-5}	6.61×10^{-10}	0.2436–0.2511	1.09–1.14	3.44–3.50	6.47–6.72
2	0.2482	1.27×10^{-4}	3.61×10^{-5}	6.33×10^{-10}	0.2184–0.2749	1.15–1.50	3.56–3.72	5.60–6.79
3b	0.2478	1.22×10^{-4}	3.62×10^{-5}	6.31×10^{-10}	0.2374–0.2772	1.15–1.34	3.49–3.76	5.86–6.99
3d	0.2521	1.39×10^{-4}	3.75×10^{-5}	6.24×10^{-10}	0.2413–0.2990	1.34–1.52	3.66–3.90	5.91–7.65
4	0.2382	1.64×10^{-4}	3.41×10^{-5}	14.5×10^{-10}	0.2206–0.2688	0.43–5.83	2.60–5.25	6.31–23.8
5	0.2656	1.96×10^{-4}	3.61×10^{-5}	18.1×10^{-10}	0.1996–0.2656	0.46–10.4	2.57–8.05	6.89–38.2
6	0.2558	1.19×10^{-4}	3.52×10^{-5}	6.54×10^{-10}	0.2496–0.2633	1.17–1.22	3.51–3.53	6.46–6.62
7	0.2586	1.22×10^{-4}	3.55×10^{-5}	6.51×10^{-10}	0.2513–0.2668	1.21–1.23	3.52–3.58	6.33–6.69
8	0.2497	1.23×10^{-4}	3.60×10^{-5}	6.88×10^{-10}	0.2356–0.2812	0.86–1.71	3.12–4.07	5.71–8.99

geneity. We explored various ways to achieve this within the numerical capabilities of the code. An energy density inhomogeneity leads to fluid flow with relativistic speeds. In run 2 we began with initial data where such flow is present already. We initialized (at $T_9\sim10$)

$$S_z=E_0\sum_{n=1}^{6}v_{zn}\cos(2n\pi z/L_{\text{grid}})\ ,$$

with $v_{zn}=0.8$, 0.4, 0.2, 0.1, 0.05, 0.025, and other quantities as in run 1. This motion with initial speeds as high as $v\sim0.6$ leads to a peak density contrast of $\delta E/E\sim2$ at $t\sim7$ s, $T_9\sim4$. The stronger inhomogeneity leads to stronger effects on the isotopes (Table II). The trace isotopes remain close to the homogeneous results as expected from adiabatic data but ^{4}He is now very inhomogeneous.

To see how the effect of inhomogeneity depends on the amplitude, we did a sequence of runs (2a–2j) where we turned up the initial inhomogeneity amplitude from zero (Fig. 1). We see that the spread between the minimum and maximum ^{4}He increases first linearly, then more slowly, whereas the average ^{4}He curves the opposite way. The effect appears to saturate at $\delta E/E\sim1$. This however is due to the complicated dependence of the evolution on the initial data. With moderate initial inhomogeneity the motion of the fluid creates a stronger inhomogeneity later on. This maximum $\delta E/E$ does not increase linearly with initial $\delta E/E$; neither does the $\delta E/E$ present later at main nucleosynthesis. Thus the runs with the largest initial $\delta E/E$ are not really much more strongly inhomogeneous.

To achieve better control of the inhomogeneity amplitude up to main nucleosynthesis, we increased the physical length of the grid to four initial horizons, and went back to $S_z=0$ initially. Thus the inhomogeneity enters the horizon later, closer to main nucleosynthesis. We show the results (runs 3a–d) in Fig. 2. The effect of inhomogeneity appears to grow roughly linearly with $\delta E/E$.

To understand the processes that affect the final abundances we look at run 3d in more detail (Figs. 3–10). From the fluid flow lines (Fig. 3) we see that the fluid stays fairly stationary at first when the inhomogeneity is still beyond the horizon. However, the energy density inhomogeneity grows (Fig. 4) until $t\sim3$ s because of inhomogeneous expansion (Fig. 5). It is a well-known result of perturbation theory that density perturbations on scales far outside the horizon will grow in a radiation-dominated cosmology.[41] Here we are of course beyond perturbation theory and not very far outside the horizon.

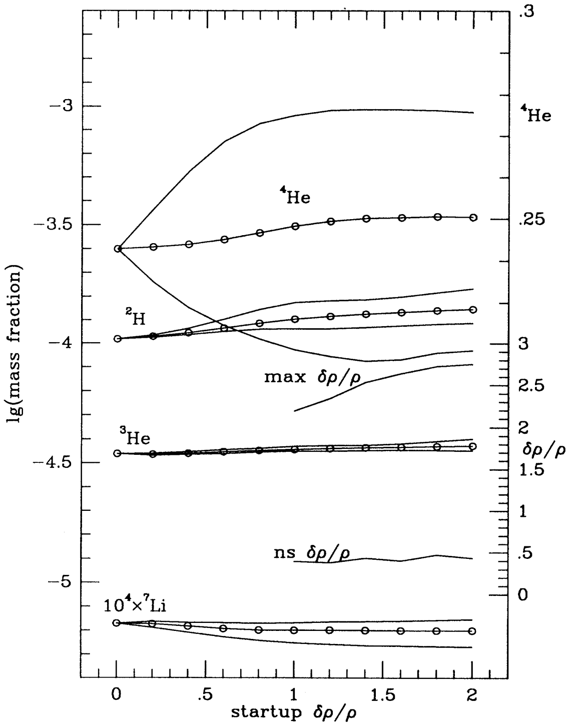

FIG. 1. The effect of increasing the initial (startup $\delta\rho/\rho$) inhomogeneity amplitude in type 2 runs (2a–2j). For each isotope we have three curves giving the maximum, average, and minimum abundances at the end of each run. The symbol "lg" in this and other figures denotes base 10 logarithm. We also plot the maximum density contrast achieved during the run (max $\delta\rho/\rho$), and the density contrast during main nucleosynthesis action (ns $\delta\rho/\rho$). In these runs increasing the initial inhomogeneity amplitude did not lead to stronger inhomogeneity at nucleosynthesis time.

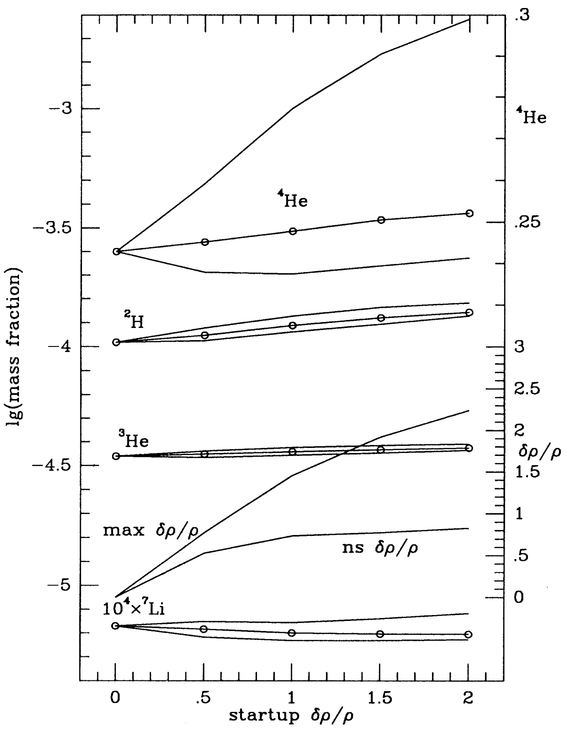

FIG. 2. The effect of increasing the initial (start-up) inhomogeneity amplitude in type 3 runs (3a–3d). The runs with a start-up inhomogeneity $\delta\rho/\rho \geq 1$ had $\delta\rho/\rho > 0.7$ at nucleosynthesis time. All abundances stay within observational limits.

The interpretation of the behavior in familiar terms suffers from the usual problems of gauge dependence. Measured in our coordinates z,t the expansion is at first ($t \leq 1$ s) faster in the center of the grid than at the edge. However, we note that the lapse function (Fig. 6) goes as high as $\alpha \sim 2$ at the center, whereas we have fixed $\alpha = 1$ at the edge. Thus at our $t = 2$ s slice, the center is actually about 3.5 s old as measured in proper time along the $z = \text{const}$ coordinate line. The proper time experienced by the fluid differs from both of these times because of fluid motion. Measured in proper time the difference in expansion rates is not as large.

Thus our statements are to be understood relative to the constant mean curvature slicing used, which defines our time coordinate t, measuring the proper time along the grid edge. At later times our models evolve to become more homogeneous and the difference in time measurements disappears.

As the inhomogeneity enters the horizon at $t \sim 10$ s, $T_9 \sim 3$ the built-up pressure difference sets the fluid into motion toward the low-density region at the center. These waves cross at $t \sim 25$ s, develop into shock waves moving at $v \sim c_s = 1/\sqrt{3}$, which travel across the grid many times colliding alternatingly at the grid center and edge. The time interval between these crossings grows with the expansion as $\sqrt{t}$. Since our plots are logarithmic in t, they do not have sufficient resolution in the time direction after $t \sim 10^3$ s.

Turning to the isotopes we see that the trace isotopes (of which ^{2}H is shown in Fig. 7) follow the temperature (Fig. 8) at early times. The nucleosynthesis begins at $T_9 \sim 0.9$. This temperature is reached first, at $t \sim 2$ min, in the center which produces 12% ^{4}He (Fig. 9) before the shock waves collide the second time at the center. This raises the temperature back to $T_9 \sim 1.1$ and stops nucleosynthesis here for the next 2 min while it begins at the edge. The final yield of ^{2}H and other trace elements is fairly homogeneous in this adiabatic run, but ^{4}He is very inhomogeneous. The grid center has produced a high ^{4}He mass fraction reaching up to 0.299 and at the edge it drops as low as 0.218. All this was achieved with

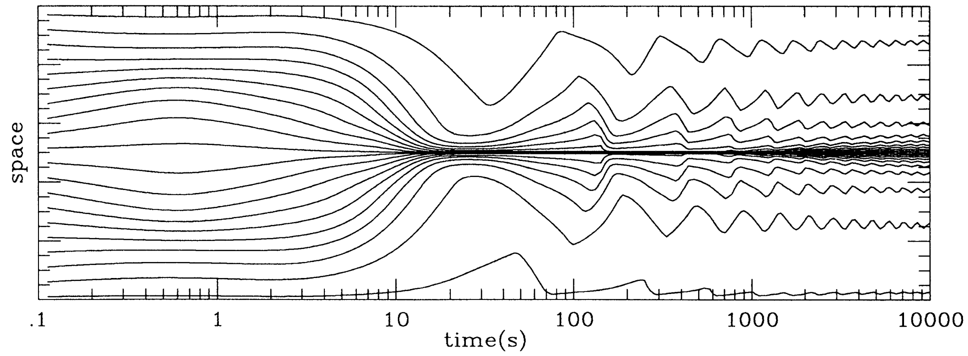

FIG. 3. Fluid flow world lines in run 3d. This is a spacetime diagram with time the horizontal (logarithmic) axis and space (z coordinate) the vertical axis. The time coordinate equals the proper time along the edge of the grid [because of periodic boundary conditions the edges (bottom and top in the figure) are identified with each other]. The code was initialized at $t \sim 0.7$ s "initial slice," but then run backward close to $t \sim 0.1$ s "first slice," where the nucleosynthesis was started. The code was then run forward somewhat past $t = 10\,000$ s, where the plot ends. The space coordinate is comoving, the grid covering 1200 present light years. This was set so that it equals four horizons, i.e., about 8 light-seconds on the initial slice ($t \sim 1$ s). The fluid is set in motion by pressure gradients when the horizon grows larger than the grid.

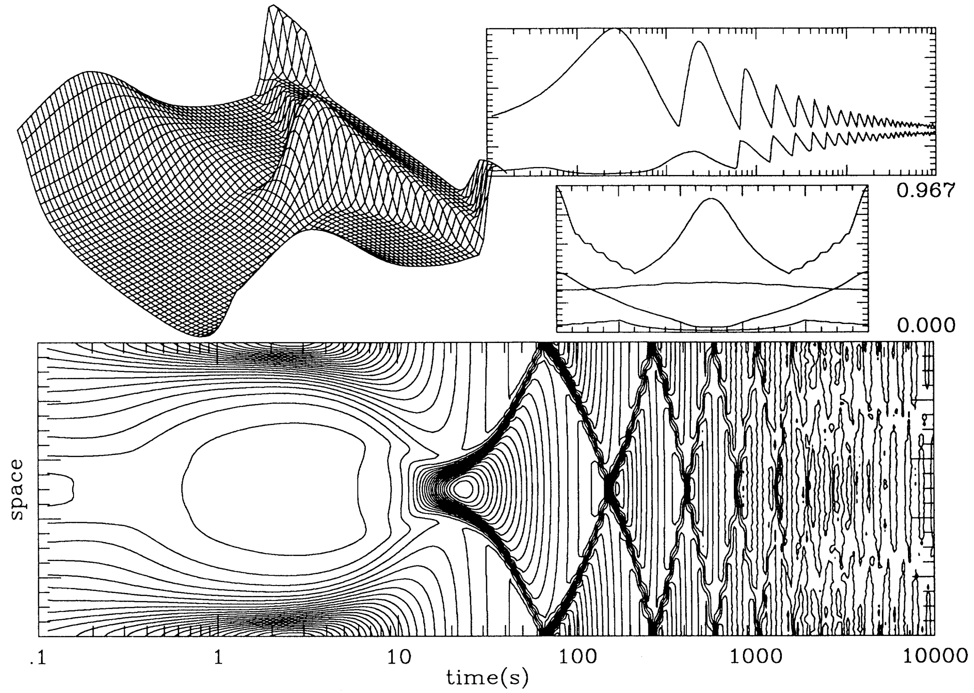

FIG. 4. The energy density in run 3d represented as a contour plot of $E/(\mathrm{tr}K)^2$. To help in reading the contour plot, it is supplemented with three smaller plots above it. On the left we have a three-dimensional plot where the section of the contour plot from 1 s to 100 s is represented as a surface revealing where the high and low values are. At top right we have a plot of the minimum and maximum as a function of time (i.e., a "side view"). The horizontal axis is the same as in the contour plot. The small tick marks on the vertical axis correspond to the contour levels of the contour plot. Below this we have a plot with the same vertical axis but the horizontal axis being the z coordinate, i.e., the same as the vertical axis of the contour plot, giving a "rear" or "front" view. We show the all-time minima and maxima of each zone, as well as the first and last (actually the $t=10\,000$ s) slice. This same scheme is used in the following figures. The two numbers to the right of the small plot give the extent of the vertical axis, which is usually from the minimum value to the maximum value; in some cases, e.g., this one, instead of the minimum, zero is used. (The minima and maxima are always taken from the whole run, which usually extends beyond the right edge of the time plots.)

$n_b/n_\gamma \sim 10^{-9.5}$ everywhere in the grid. This variation reflects the n abundance (Fig. 10) available before nucleosynthesis.

Throughout this work we notice one behavior for the trace isotopes ^{2}H, ^{3}He, and ^{7}Li, and another for ^{4}He. The trace isotopes are chiefly determined by the n_b/n_γ ratio during main nucleosynthesis and will thus be strongly affected only by nonadiabatic inhomogeneities. They are rather oblivious to the previous history of the Universe. The ^{4}He is different, since it is determined by the n mass fraction available at main nucleosynthesis, and the survival of neutrons till this time depends on previous circumstances. Thus we have to survey the prenucleosynthesis history of the Universe to explain the ^{4}He production.

In the adiabatic case the nucleosynthesis begins everywhere at the same temperature. But we note that the average yield of ^{4}He has been raised in all our adiabatic runs, compared to the homogeneous case. Why did more neutrons survive?

Review the history of the neutron fraction in standard nucleosynthesis.[42] At high temperature neutrons follow their equilibrium abundance. As the temperature falls, the rates of the weak $n \leftrightarrow p$ reactions drop very rapidly and the n fraction is left behind (above) the decreasing equilibrium abundance, and freezes at a certain value. As the time scale grows, the n fraction again begins to go down, now due to the free decay of neutrons; but then the nucleosynthesis begins.

The free decay of neutrons depends on the proper time experienced by them. In our runs the matter is flowing at relativistic speeds. Time dilation thus causes neutrons to live longer and thus more survive until nucleosynthesis. We measured this effect in run 2 by disabling the time dilation of nuclear reactions in the code. In turned out that time dilation accounted for about one-third of the total increase in ^{4}He in this run.

The larger effect is that of the temperature history. The highest ^{4}He production occurred in the grid center in run 3d (Fig. 9). We note that this is the region with lower energy density, and thus lower temperature, at $t < 10$ s. At early times ($t \lesssim 0.5$ s) the n abundance is at equilibrium, meaning that n is low where T is low. This however is not relevant, since all regions go through the same values of T before reaching the nucleosynthesis temperature. What matters is the rate at which temperature falls as the weak reactions drop out of equilibrium and the n abundance freezes. The low-density regions go

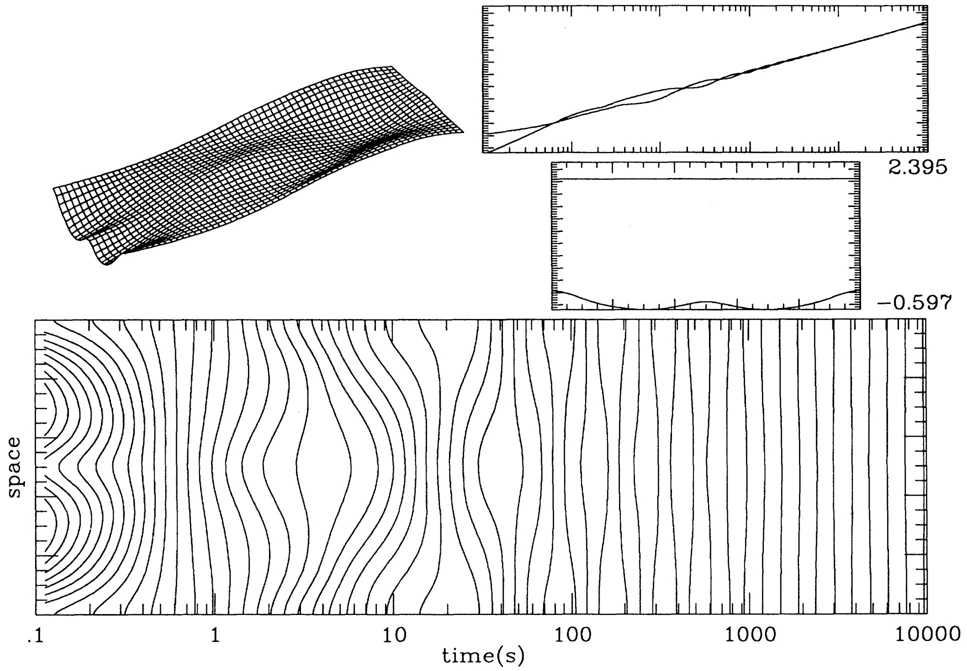

FIG. 5. The expansion represented by the logarithm of the metric component A, in run 3d. A is normalized to 1 ($\lg A = 0$) at the initial slice, which lies at $t \sim 0.7$ s. Each contour level corresponds to expansion by a factor of 1.122 (length). The total expansion in the run is about 10^3, i.e., almost 10^9 in volume. (The run actually extended past the right edge of the plot, so that $\lg A = 2.395$ at the end of the run, but ~ 2.05 at the $t = 10\,000$ s slice.) The surface plot is shown from a lower perspective to make the inhomogeneity easier to see.

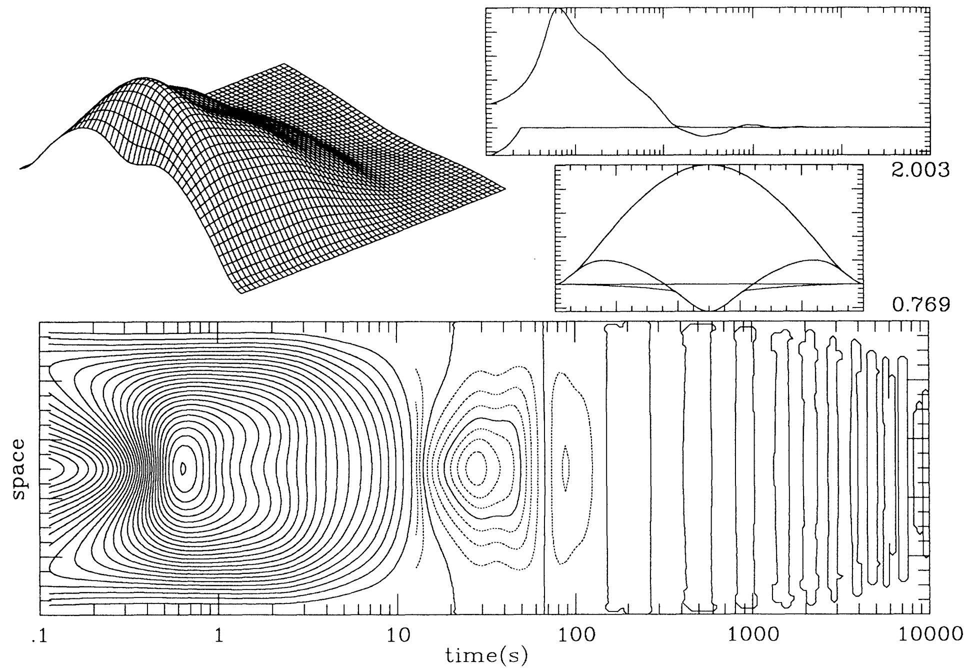

FIG. 6. The lapse function α in run 3d. The contour interval is 0.04, with supplemental 0.01 contours (broken lines) after $t \approx 13$ s. After $t = 100$ s, the lapse is rather homogeneous, $\alpha \approx 1$, but the $\alpha = 1$ contour keeps showing up.

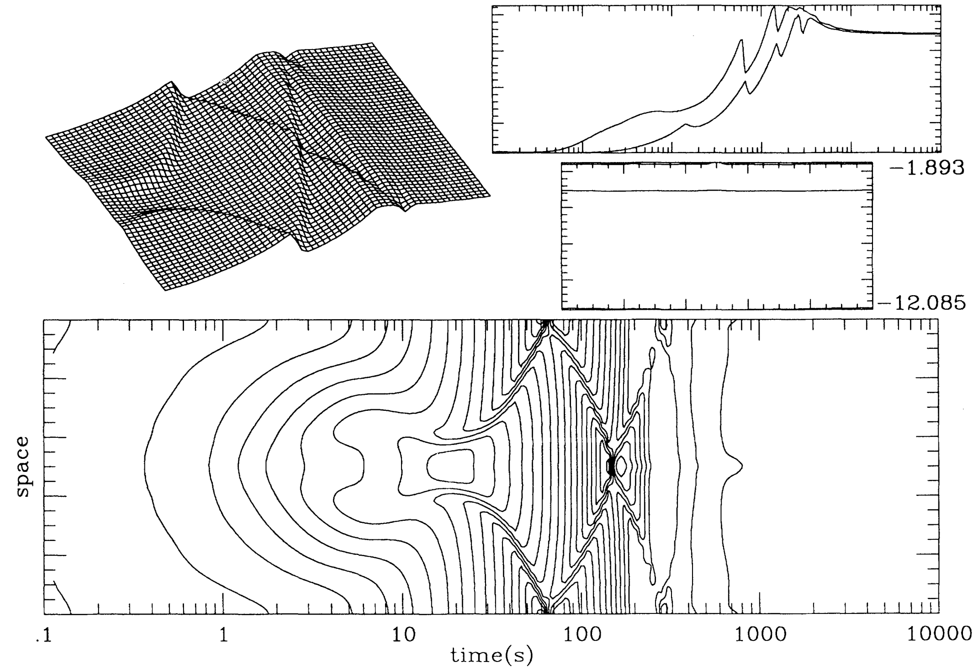

FIG. 7. The deuterium mass fraction in run 3d. We have plotted lg^{2}H, and the surface plot is now from $t=10$ s to $t=1000$ s, covering the nucleosynthesis. The final ^{2}H is very homogeneous in this adiabatic run. The contour interval is 0.5.

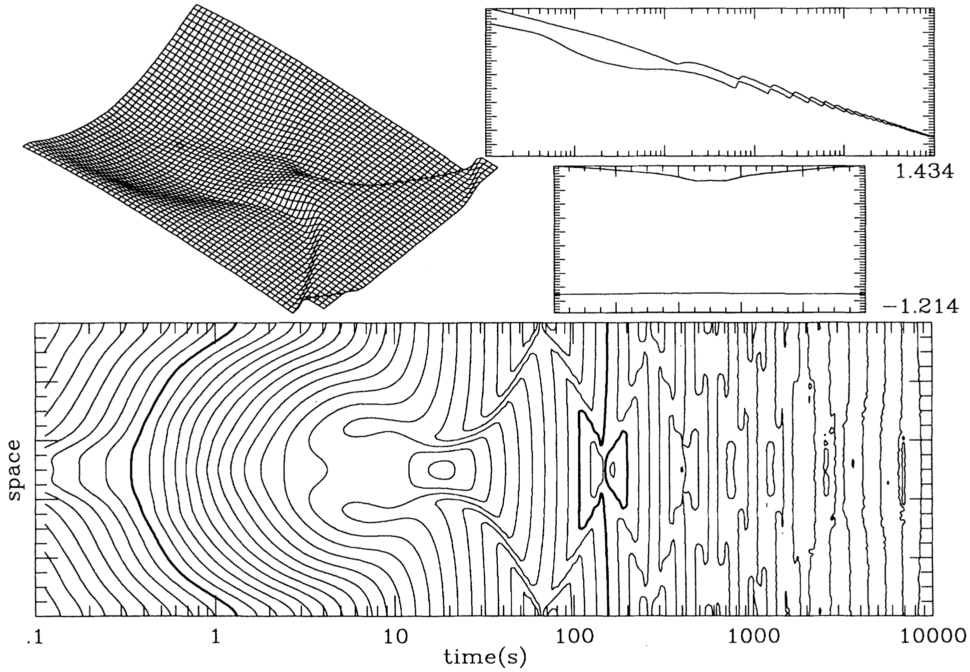

FIG. 8. The temperature in run 3d. The function plotted is lgT_9. The contour interval is 0.05, i.e., cooling by a factor 1.122. $T_9=10$ and $T_9=1$ are shown as thicker lines. The surface plot is from $t=1$ s to $t=100$ s.

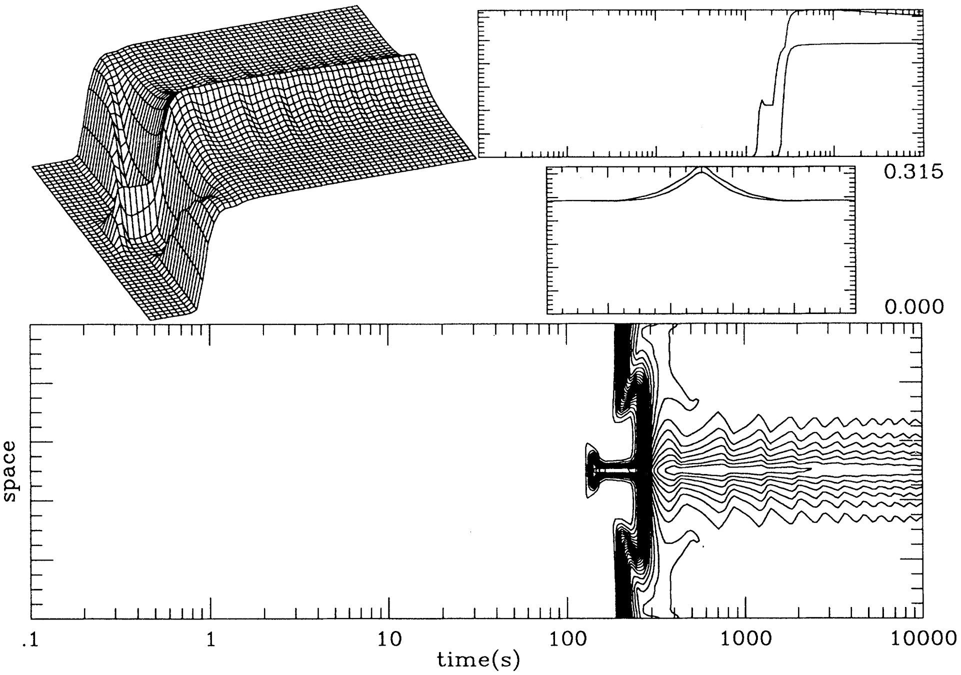

FIG. 9. The ^{4}He mass fraction in run 3d. The contour interval is 0.01 and the surface plot is from $t = 100$ s to $t = 10\,000$ s.

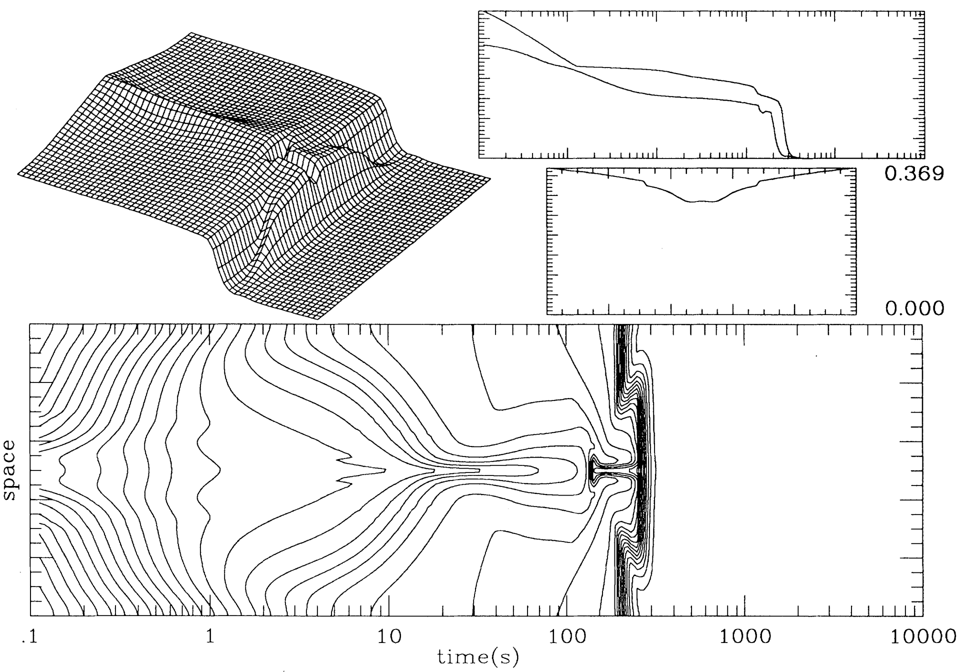

FIG. 10. The neutron mass fraction in run 3d.

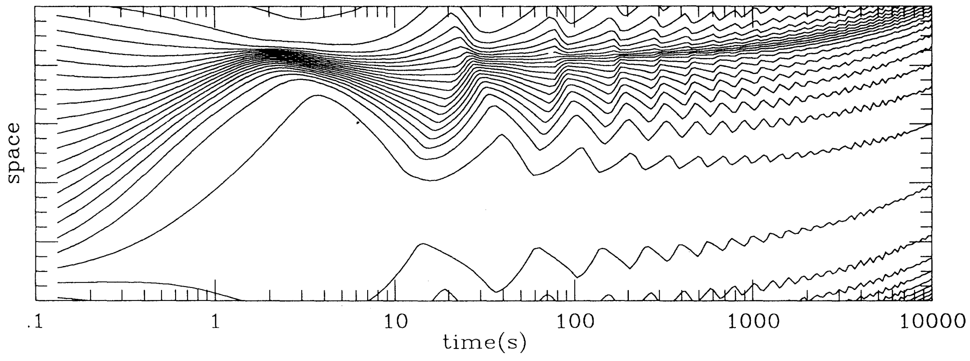

FIG. 11. Fluid flow world lines in runs 2, 4, and 5. The grid covers 600 present light years.

through these temperatures earlier when the expansion rate is higher; thus T falls faster and n freezes at a higher level. Later the central region is heated up as energy flows in, but this happens at a temperature too low to alter the neutron profile. If the early temperature profile had been retained long enough the opposite effect would have taken place around the edge. But when the hot edge region finally approaches freeze-out temperatures, the inhomogeneity has already entered the horizon and energy flows out of the edge region accelerating the cooling.

If the scale of inhomogeneity had been much larger than the horizon, there would not have been such an effect, because the local expansion rate would have been determined by the local energy density only; i.e., different zones would have behaved like independent homogeneous universes, and with the same n_b/n_γ they would have produced the same abundances. We are studying precisely the interesting scale where only a numerical relativity code can reveal what happens.

Although the maximum ^{4}He is very high, the average ^{4}He is raised only by 0.01 above the homogeneous result. This is because most nucleons were in the low ^{4}He producing region.

In run 2 (Figs. 11–15) the geometric effects were weaker since the scale was smaller; i.e., the inhomogeneity enters the horizon earlier. Other effects appear since we have set the fluid moving from the beginning. Again we have very inhomogeneous ^{4}He production (Fig. 15), reflecting the n profile at the onset of nucleosynthesis. The highest ^{4}He production is again at grid center. From

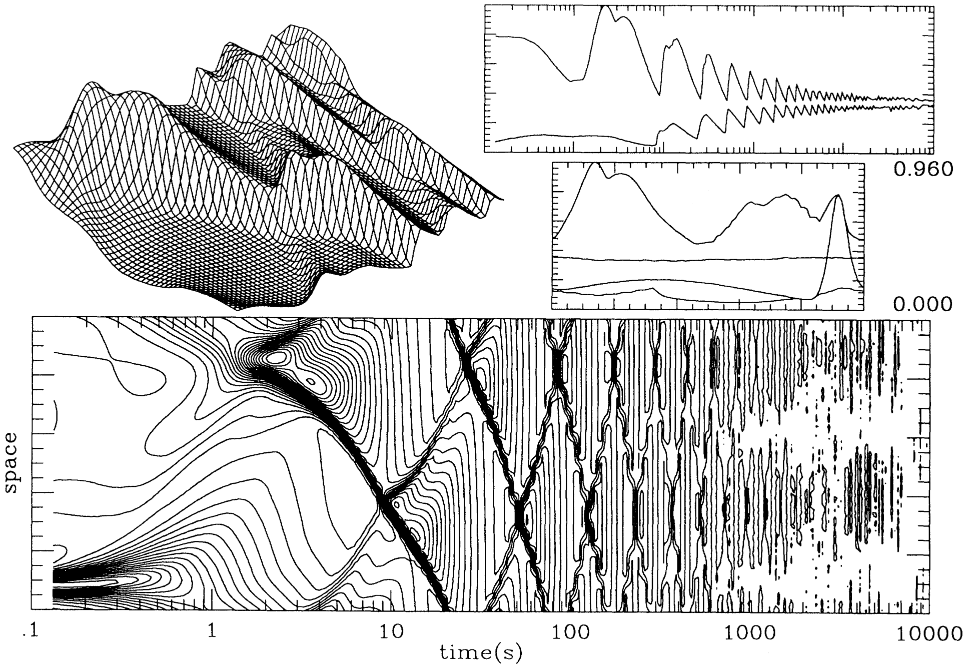

FIG. 12. $E/(\mathrm{tr}K)^2$ in runs 2, 4, and 5. The surface plot is from $t=1$ s to $t=100$ s.

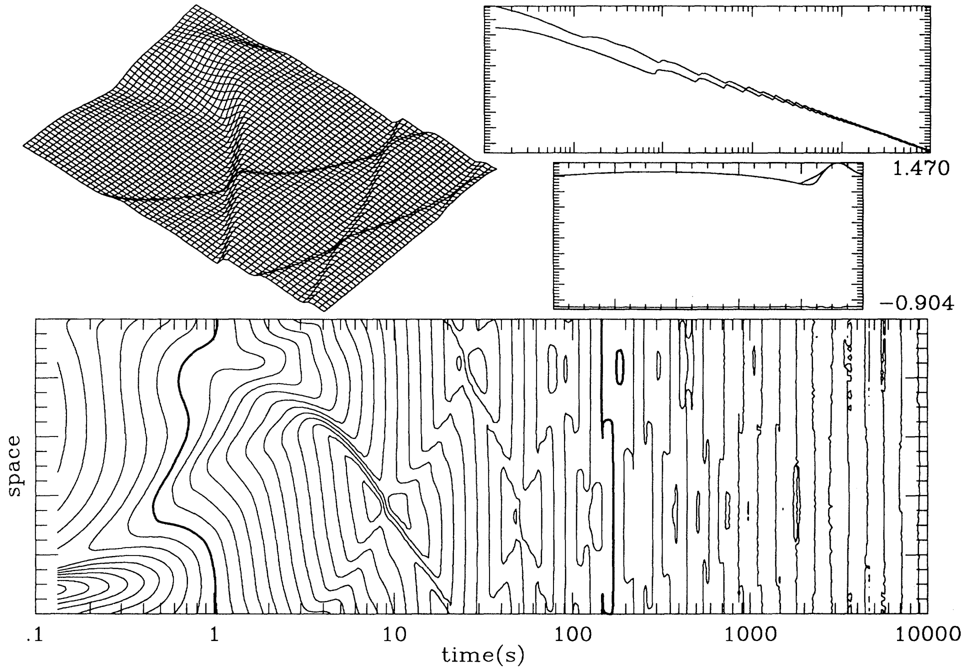

FIG. 13. The temperature in runs 2, 4, and 5. Compare to Fig. 8.

the flow lines (Fig. 11) we see that these neutrons came originally from the right half of the grid. Because of energy flowing out of this region, temperature drops here more rapidly, leaving the *n* fraction (Fig. 14) frozen at a higher value. In the other half the opposite happens; the inflow of energy slows down the cooling, delaying the freeze-out, and bringing the neutron fraction to a lower value. Because more nucleons were in the first half the average ^{4}He production went up.

In runs 4 and 5 we study the effect of a nonadiabatic inhomogeneity. Other quantities except the baryon density D (Figs. 16 and 17) are set as in run 2, so that these

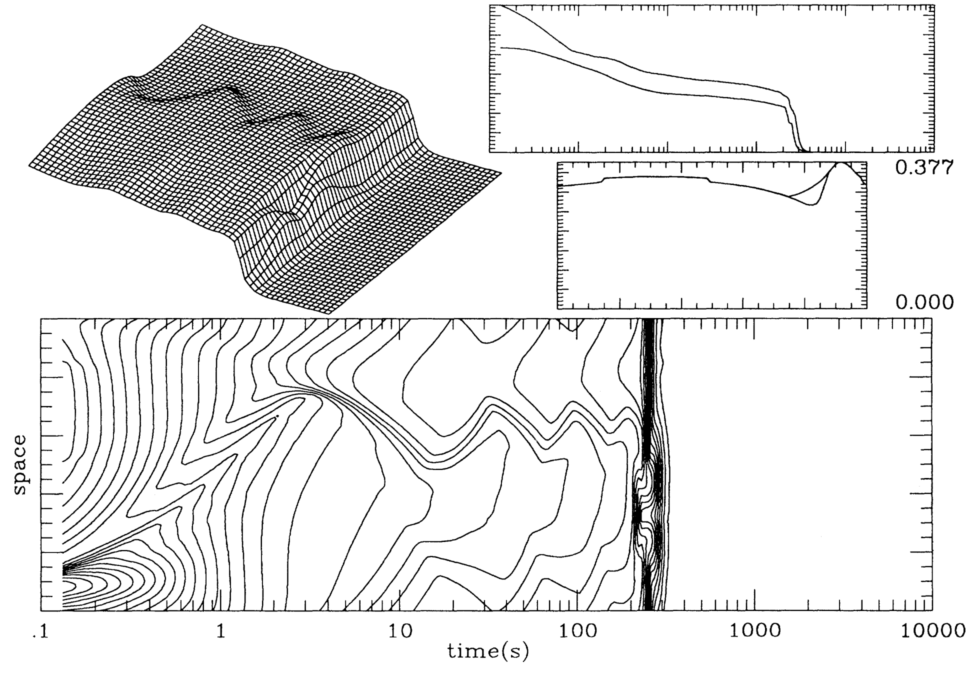

FIG. 14. The neutron mass fraction in run 2.

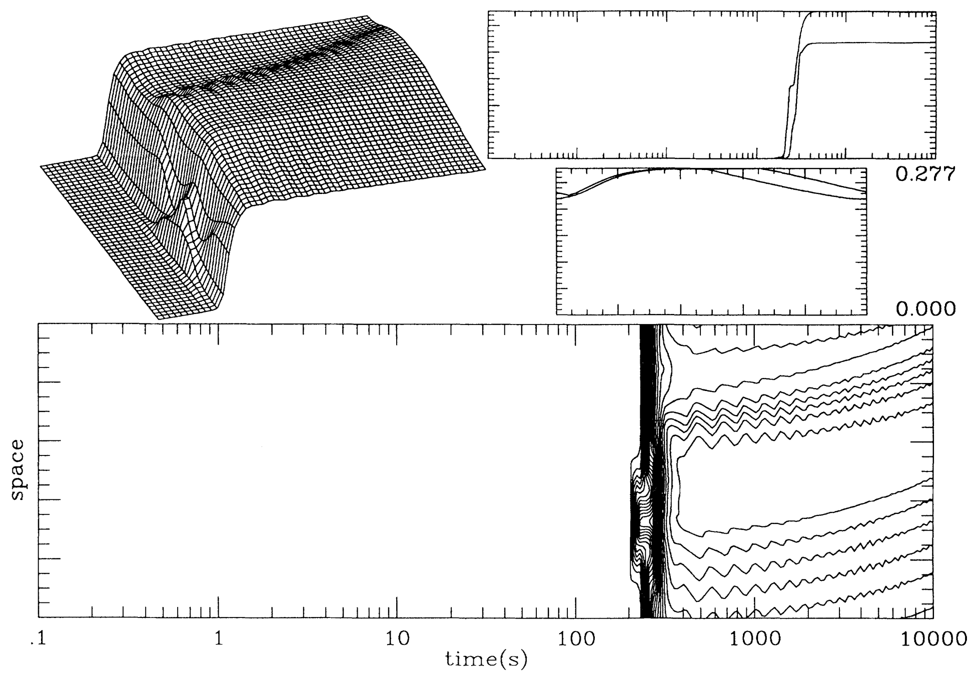

FIG. 15. The ^{4}He mass fraction in run 2.

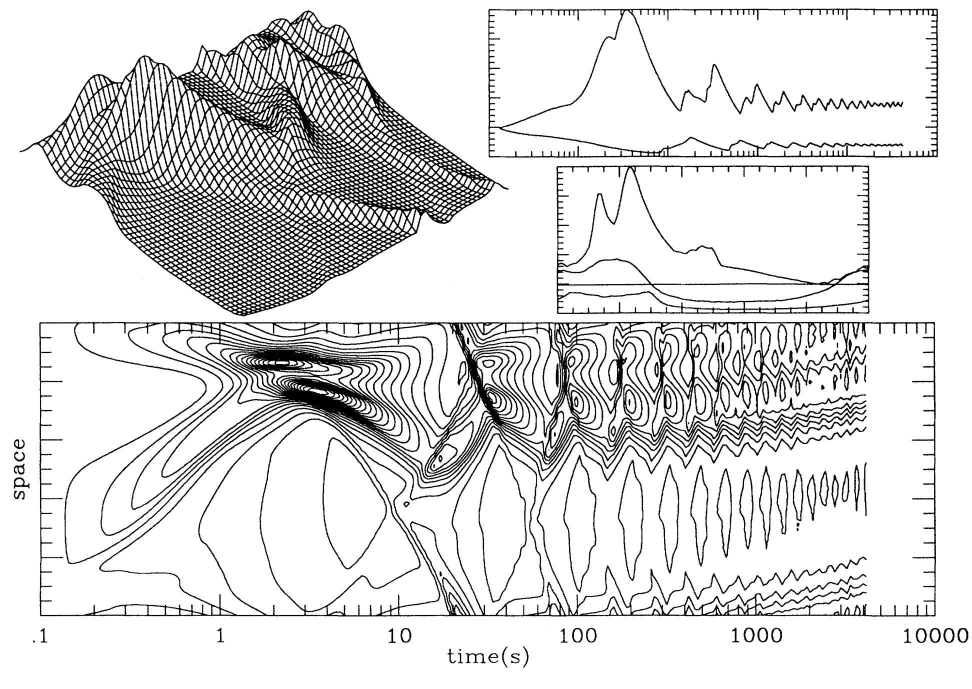

FIG. 16. The baryon density in the nonadiabatic run 4. The quantity plotted is $D/(\mathrm{tr}K)^{3/2}$. Energy density in this run is as in Fig. 12, but the baryon density was set constant on the first slice.

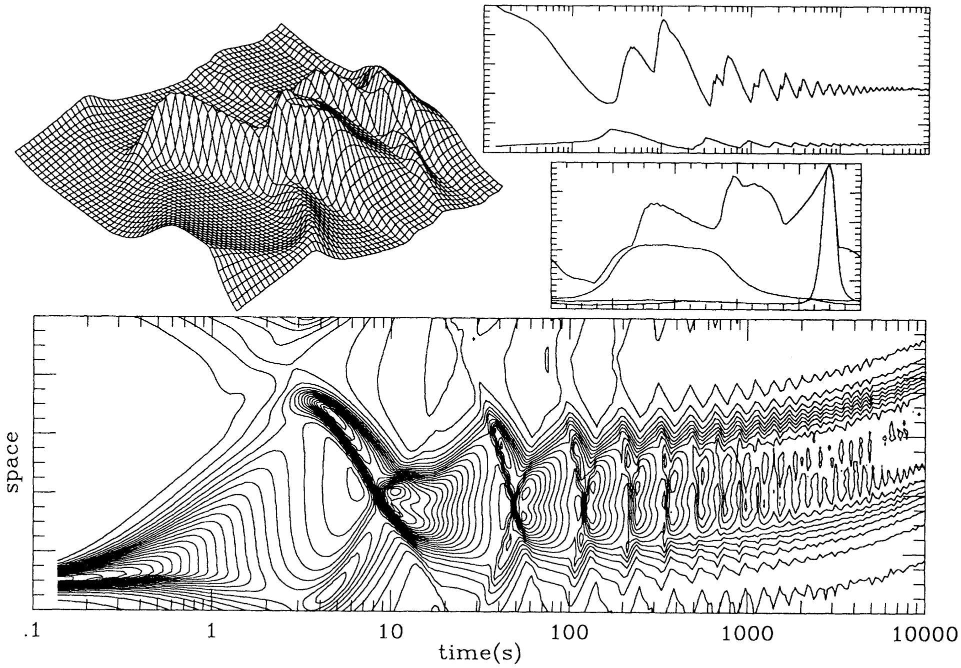

FIG. 17. The baryon density in run 5.

runs have the same geometry and radiation fluid behavior (Figs. 11–13). In run 4 D is set constant in the first slice ($T_9 \sim 20$). The best way to view this is an inhomogeneity in n_b/n_γ, or D/E, since E is inhomogeneous. D is set so that the average n_b/n_γ remains $10^{-9.5}$. Because the baryons follow the fluid flow, D will not stay constant after the first slice. The fluid flow lines (Fig. 12) show that the initial low-energy-density region covering most of the first slice is squeezed into the left (or top) half of the grid, increasing the comoving baryon density there and reducing it in the right half.

The effect of the n_b/n_γ inhomogeneity is now seen in the trace isotopes. High n_b/n_γ leads to low ^{2}H, ^{3}H, ^{3}He, and ^{7}Li, and to high ^{7}Be (Figs. 18–20). The final ^{7}Li is the sum of ^{7}Li and ^{7}Be and since $n_b/n_\gamma = 10^{-9.5}$ is close to its minimum, the final ^{7}Li is raised in both high- and low-density regions, raising the average by over a factor of 2 from the homogeneous result. The average ^{2}H is raised and ^{3}He is lowered. This is the usual effect of n_b/n_γ inhomogeneity as obtained in homogeneous spacetimes.

But its usual effect is to raise the average ^{4}He, whereas the result of run 4 is to lower it by 0.010 from run 2 with homogeneous n_b/n_γ, and by 0.005 from the completely homogeneous run. The ^{4}He abundance profile (Fig. 21) does not follow n_b/n_γ as the trace isotopes do, manifesting that ^{4}He depends on different physics. Indeed it is close to the adiabatic run 2 (Fig. 15). Since the prenucleosynthesis n/p history depends only on the proper time temperature history of the fluid and is independent of the baryon density, the n evolution up to the time of nucleosynthesis is identical in both runs; they differ only in the baryon density profile. As nucleosynthesis begins, the difference in baryon density shows by causing nucleosynthesis to begin earlier, at a higher temperature, in the region of high baryon density, thus raising the ^{4}He abundance there. Since this region by chance happens to correspond to a low n abundance, the minimum ^{4}He is raised, and similarly the maximum ^{4}He is lowered from the adiabatic run 2. This effect is small compared to the effect of n history, so that the final ^{4}He profile is not very different from run 2. However the average is changed since the regions now have different baryon densities and get weighted differently in averaging.

The surprising result of reduced ^{4}He production is now explained by the high baryon density and the low ^{4}He being located in the same region. This is completely fortuitous since these two are largely independent. Thus if we are allowed to independently set the initial n_b and n_γ profiles we can use this freedom to adjust the final average ^{4}He by setting most baryons in a low or high ^{4}He producing region.

We demonstrate this in run 5, which is identical to runs 2 and 4 except for the baryon density (Fig. 17) which we have set so that high-baryon density falls in the high-n fraction region in the center of the grid at nucleosynthesis time (we achieved this by setting D homogeneous at $T_9 \sim 5$). Our effort is rewarded with a large increase in total ^{4}He production, 0.027 higher than in run 4. The ^{4}He abundance profiles in these runs are fairly similar, the average just gets weighted differently.

There remains an unused inhomogeneity freedom in

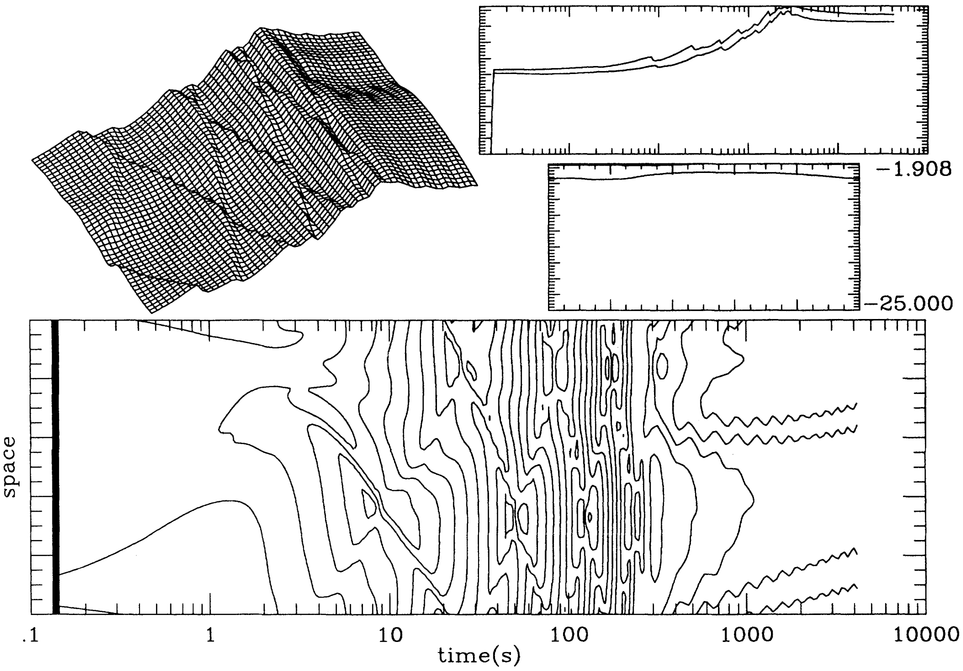

FIG. 18. The deuterium mass fraction in run 4 (nonadiabatic). Compare to Fig. 7.

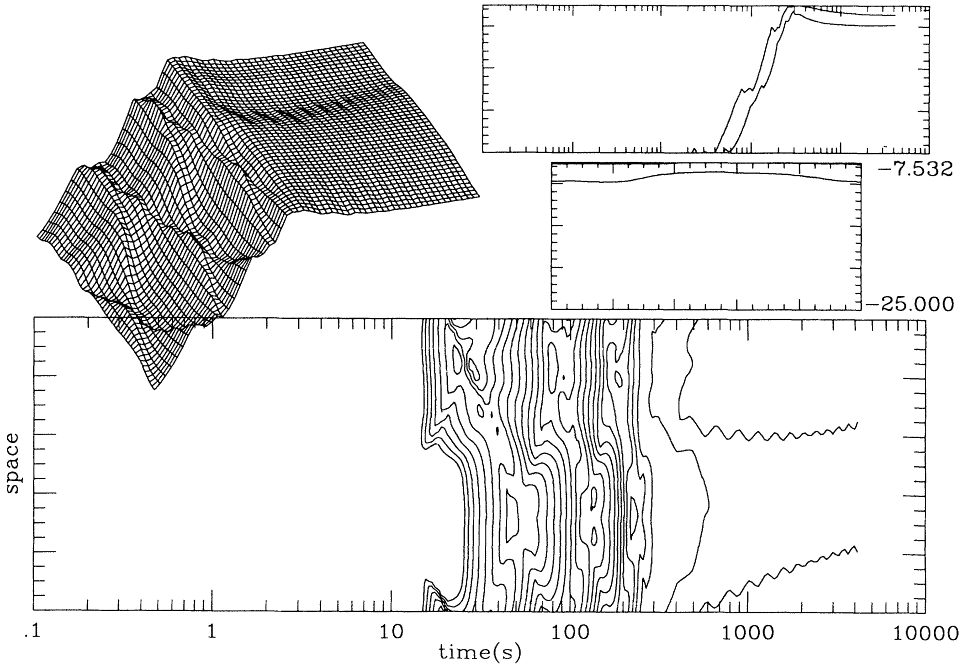

FIG. 19. ^{7}Li in run 4. The lowest contour line is 10^{-31}.

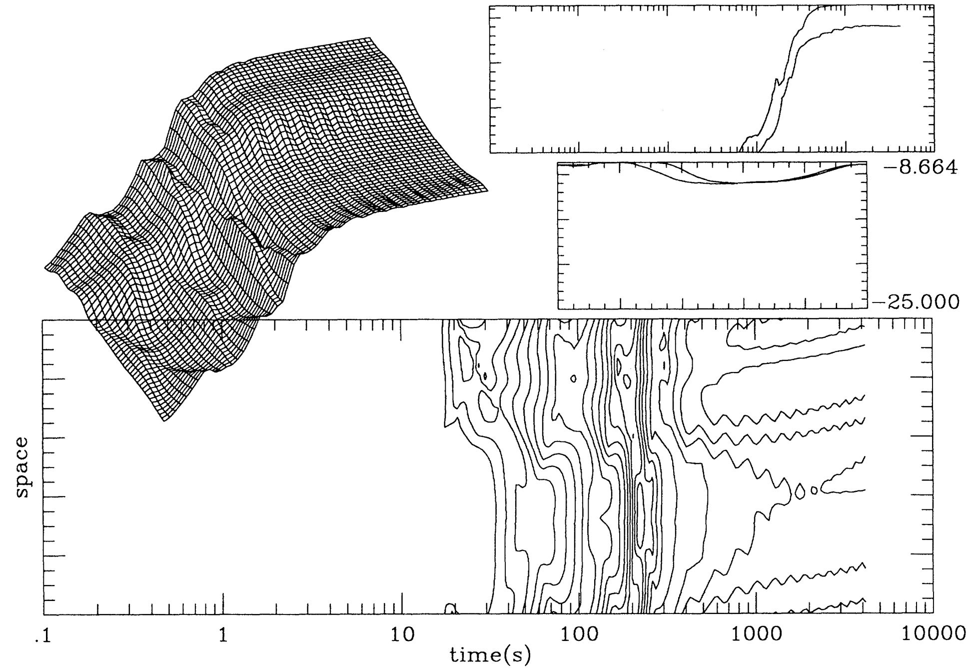

FIG. 20. ^{7}Be in run 4.

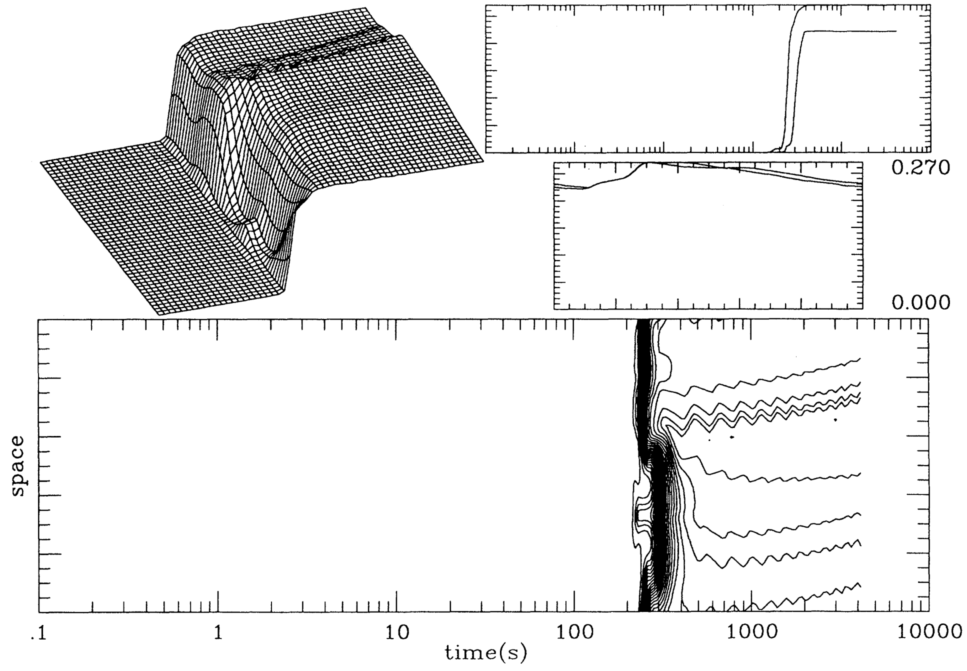

FIG. 21. ^{4}He in run 4.

setting the curvature. The curvature of spacetime is related to but not uniquely determined by the energy-momentum density, allowing for the presence of gravity waves. This freedom in setting the initial data is represented by our extrinsic curvature component K_1, which gives the difference in expansion rates along x and y directions, i.e., anisotropic expansion. In run 6 we initialize at $T_9 \sim 10$ with inhomogeneous K_1:

$$K_1 = \sum_{n=1}^{6} K_{1n}\cos(2\pi n z/L_{\text{grid}})$$

with $K_{1n}=1$, 0.5, 0.25, 0, 0, 0. This disturbance in the curvature of spacetime propagates as two waves running in opposite directions (Fig. 22). These are essentially long-wavelength gravitational waves. On our start-up slice we initialize $S_z=0$, E and D homogeneous, thus $n_b/n_\gamma=$const. Adjusting the energy density on the start-up slice leads to a mildly inhomogeneous energy density. Thus we fail to achieve pure initial K_1 inhomogeneity. Inhomogeneous K_1 leads to inhomogeneous expansion (Fig. 23). This creates (further) energy density inhomogeneity, and therefore fluid motion. The two disturbances propagate at different speeds, the K_1 disturbance at the speed of light, the density disturbance at the speed of sound, $c_s = 1/\sqrt{3}$. The flow velocities are small.

The isotope production is very homogeneous as can be expected from adiabatic data. The inhomogeneity in ^{4}He reflects the high n/p ratio in the center of the grid which seems to be due to the earlier temperature drop in this region because of inhomogeneity in E. Compared to the homogeneous case or the run with an adiabatic density inhomogeneity, the trace isotopes have remained the same but ^{4}He is up. This is due to the faster expansion because of the K_1^2 contribution to the expansion rate. In run 7 we increased this contribution by adding short-wavelength terms into the initial K_1: $K_{1n}=1$, 0.5, 0, 0, 0.5, 0.5. Other isotopes remained the same but ^{4}He was further increased by 0.005.

Run 8 was like run 3b, but with nonadiabatic density inhomogeneity; i.e., D was again set constant at the first slice, leading to inhomogeneities in the trace isotopes; the effect was not however as large as in the runs with initial fluid velocities (runs 4 and 5).

The preceding runs were for an average baryon density $\eta = 10^{-9.5}$, which is the value favored by standard nucleosynthesis. We repeated runs 2, 4, 5, and 7 for $\eta = 10^{-10}$, 10^{-9}, and $10^{-8.5}$. The results are presented in Fig. 24. The runs homogeneous in n_b/n_γ show a dependence on η similar to the standard model. Changing η changes the time of nucleosynthesis and thus a dynamically inhomogeneous model is caught in a slightly different stage. This explains the small differences in the shapes of the yield curves. Adding n_b/n_γ inhomogeneity introduces averaging over a range of baryon-to-photon ratios and has the most remarkable effect where the yield curve is most curved. Thus the ^{7}Li minimum at $\eta = 10^{-9.5}$, which is retained in adiabatic models, is washed away in the nonadiabatic runs.

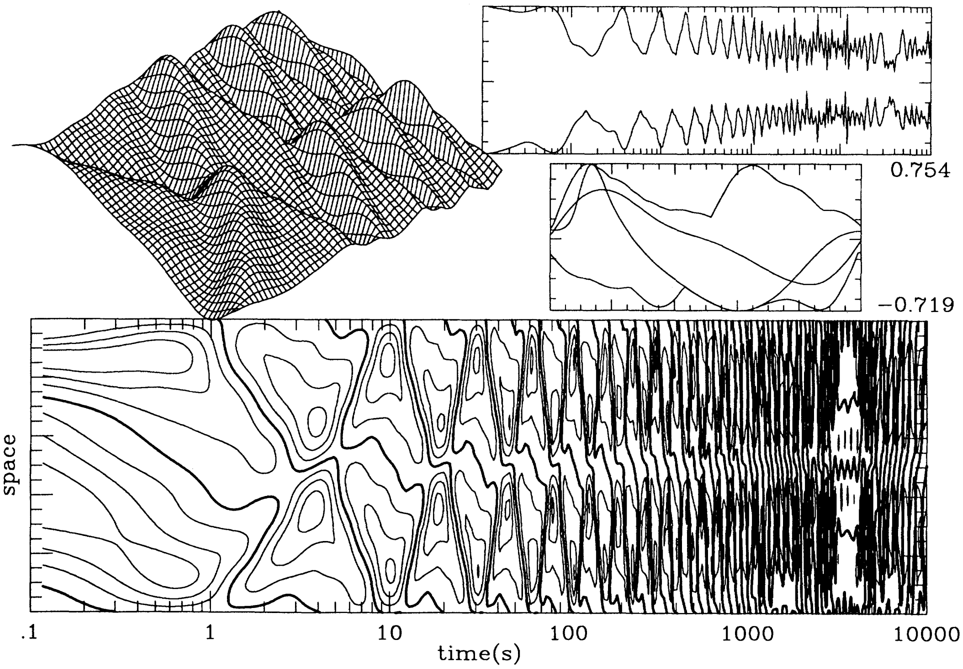

FIG. 22. $K_1/\mathrm{Tr}K$ in run 6. The surface plot is from $t=1$ s to $t=100$ s.

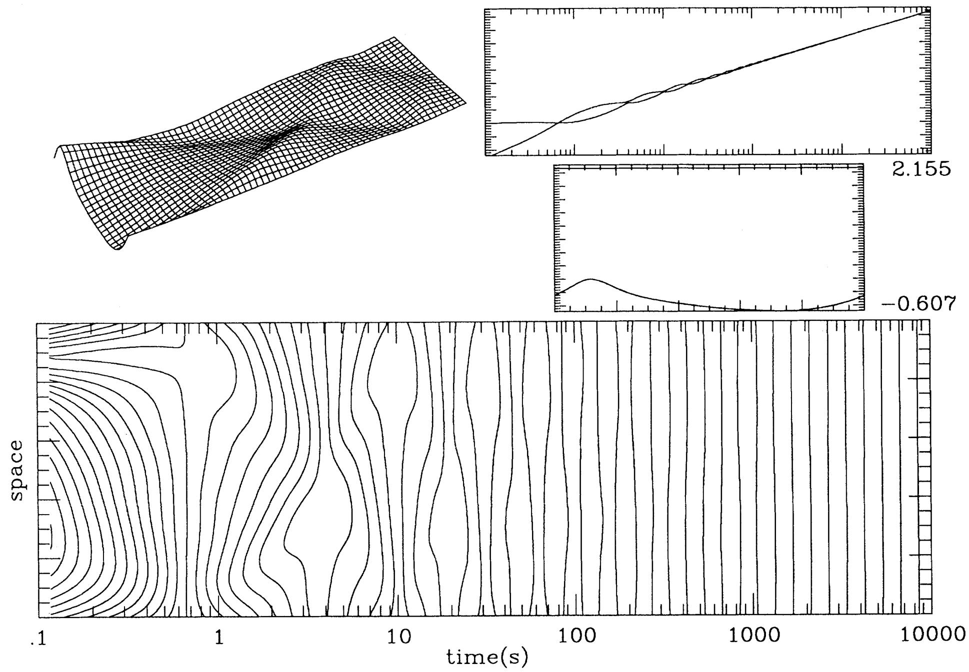

FIG. 23. lg$A$ in run 6. Compare to Fig. 5. The surface plot is from t=0.2 s to t=20 s.

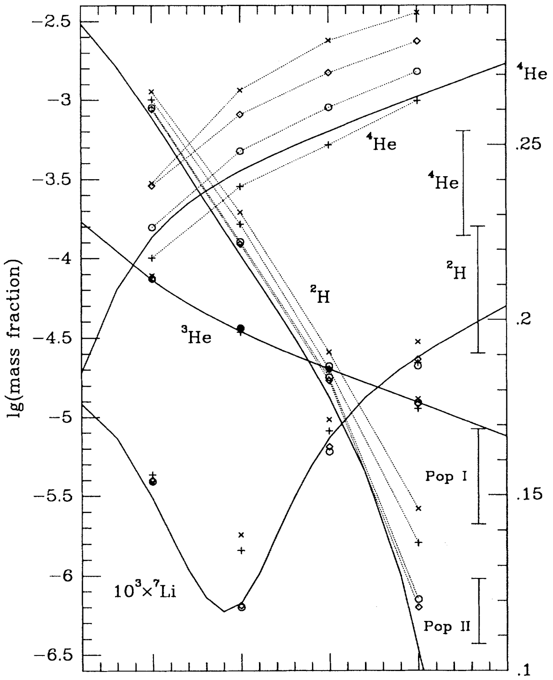

FIG. 24. The dependence of the isotope yields on η in our inhomogeneous models. Each type (○ =2, + =4, × =5, ◇=7) of inhomogeneous model was run with four values on η. The standard model (solid curves) is shown for comparison. The observational limits for ^{4}He, ^{2}H, and ^{7}Li (Pop I and II) are indicated on the right. The broken lines connect yields from runs of the same type but with different η (^{2}H and ^{4}He only). In the adiabatic runs (2 and 7) only ^{4}He is significantly different from the standard model.

IV. CONCLUSIONS

We have studied primordial nucleosynthesis with horizon-scale curvature inhomogeneities. We conclude that strong ($\delta\rho/\rho \sim 1$) inhomogeneities are allowed by the observed primordial abundances (see, e.g., Fig. 2). Adiabatic energy-density inhomogeneities (n_b/n_γ=const) have a significant effect on ^{4}He only. This is because ^{4}He depends on the number of neutrons that have survived until nucleosynthesis densities and temperatures, which in turn depends on the preceding dynamical history. In contrast, the other isotope yields are determined by the baryon-to-photon ratio n_b/n_γ at nucleosynthesis and are strongly affected by nonadiabatic ($n_b/n_\gamma \neq$const) inhomogeneities only.

The usual effect of all kinds of inhomogeneities is to raise both ^{2}H and ^{4}He. This narrows the range of η allowed by the observational upper limits. (The upper limit for η from the lower limit for ^{2}H is relaxed but gets replaced by the ^{4}He limit.) In the case of a strong nonadiabatic inhomogeneity, η should be somewhat larger than $10^{-9.5}$ to avoid ^{2}H overproduction. It is difficult to lower the ^{4}He yield with inhomogeneity. All three basic kinds of inhomogeneities, isocurvature n_b/n_γ inhomogeneity and the two adiabatic curvature inhomogeneities—energy-density inhomogeneity and anisotropic expansion inhomogeneity (long gravitational waves), when applied alone, raise it. However, we demonstrated that by combining n_b/n_γ inhomogeneity and energy-density inhomogeneity in a nonadiabatic curvature inhomogeneity it is indeed possible to reduce the ^{4}He yield below the standard-model result. This would make larger values of η acceptable. This requires somewhat of a conspiracy concentrating the highest baryon densities in those regions where the fluid motion and geometry lead to the lowest ^{4}He yields. In general, higher ^{4}He is the more likely result.

Nonadiabatic inhomogeneities wash away the ^{7}Li minimum at $\eta \sim 10^{-9.5}$. If the Population II value is the true primordial ^{7}Li abundance, this rules out strongly nonadiabatic inhomogeneities in the nucleosynthesis era. The Population I value on the other hand can be produced in a wide range of η, giving no relevant constraint. Adiabatic inhomogeneities keep the low ^{7}Li minimum so they are compatible with the ^{7}Li of both populations.

ACKNOWLEDGMENTS

This work was partially supported by National Science Foundation Grants Nos. PHY84-51732, PHY84-04931, PHY87-06315, and PHY88-06567; and performed in part under the auspices of the U.S. Department of Energy by the Lawrence Livermore National Laboratory under Contract No. W-7405-ENG-48. The computations were performed on a Cray X-MP/48 at the National Center for Supercomputing Applications at the University of Illinois at Urbana–Champaign.

---

*Present address.

[1] J. Yang, M. S. Turner, G. Steigman, D. N. Schramm, and K. A. Olive, Astrophys. J. **281**, 493 (1984).

[2] A. M. Boesgaard and G. Steigman, Annu. Rev. Astron. Astrophys. **23**, 319 (1985).

[3] A recent discussion of the standard big-bang nucleosynthesis is given by K. A. Olive, D. N. Schramm, G. Steigman, and T. P. Walker, Phys. Lett. B **236**, 454 (1990). They use $\tau_n = 889.8$ s and the same reaction rates as we do, and compare to an observational value $^4\mathrm{He} = 0.23 \pm 0.01$.

[4] G. R. Caughlan and W. A. Fowler, At. Data Nucl. Data Tables **40**, 283 (1988).

[5] Particle Data Group, G. P. Yost *et al.*, Phys. Lett. B **204**, 1 (1988).

[6] B. E. J. Pagel, in *Inner Space/Outer Space: The Interface Between Cosmology and Particle Physics,* proceedings of the Workshop, Batavia, Illinois, 1984, edited by E. W. Kolb *et al.* (University of Chicago, Chicago, 1986), p. 72.

[7] E. R. Harrison, Astron. J. **73**, 533 (1968).

[8] R. V. Wagoner, Astrophys. J. **179**, 343 (1973).

[9] G. R. Gisler, E. R. Harrison, and M. J. Rees, Mon. Not. R. Astron. Soc. **166**, 663 (1974).

[10] R. I. Epstein and V. Petrosian, Astrophys. J. **197**, 281 (1975).

[11] Ya. B. Zel'dovich, Pis'ma Astron. Zh. **1**, 10 (1975) [Sov. Astron. Lett. **1**, 5 (1975)].

[12] D. W. Olson and J. Silk, Astrophys. J. **226**, 50 (1978).

[13] J. D. Barrow and J. Morgan, Mon. Not. R. Astron. Soc. **203**, 393 (1983).

[14] K. E. Sale and G. J. Mathews, Astrophys. J. **309**, L1 (1986).

[15] E. W. Kolb and M. S. Turner, *The Early Universe* (Addison-Wesley, Reading, MA, 1990), Sec. 9.2.3.

[16] J. Centrella, R. A. Matzner, T. Rothman, and J. R. Wilson, Nucl. Phys. **B266**, 171 (1986).

[17] J. Centrella and J. R. Wilson, Astrophys. J. **273**, 428 (1983).

[18] J. Centrella and J. R. Wilson, Astrophys. J. Suppl. Ser. **54**, 229 (1984).

[19] T. Rothman and R. Matzner, Phys. Rev. D **30**, 1649 (1984).

[20] H. Kurki-Suonio and R. Matzner, Phys. Rev. D **31**, 1811 (1985).

[21] J. W. York, in *Sources of Gravitational Radiation,* edited by L. L. Smarr (Cambridge University Press, Cambridge, England, 1979), p. 83.

[22] J. R. Wilson, in *Sources of Gravitational Radiation* (Ref. 21), p. 423.

[23] E. Witten, Phys. Rev. D **30**, 272 (1984).

[24] J. H. Applegate and C. J. Hogan, Phys. Rev. D **31**, 3037 (1985).

[25] J. H. Applegate, C. J. Hogan, and R. J. Scherrer, Phys. Rev. D **35**, 1151 (1987).

[26] C. Alcock, G. M. Fuller, and G. J. Mathews, Astrophys. J. **320**, 439 (1987).

[27] J. H. Applegate, C. J. Hogan, and R. J. Scherrer, Astrophys. J. **329**, 572 (1988).

[28] G. Fuller, G. Mathews, and C. Alcock, Phys. Rev. D **37**, 1380 (1988).

[29] H. Kurki-Suonio, Phys. Rev. D **37**, 2104 (1988).

[30] R. A. Malaney and W. A. Fowler, Astrophys. J. **333**, 14 (1988).

[31] N. Terasawa and K. Sato, Phys. Rev. D **39**, 2893 (1989).

[32] C. Alcock, G. M. Fuller, G. J. Mathews, and B. Meyer, Nucl. Phys. **A498**, 301c (1989).

[33] H. Kurki-Suonio, R. A. Matzner, J. M. Centrella, T. Rothman, and J. R. Wilson, Phys. Rev. D **38**, 1091 (1988).

[34] H. Kurki-Suonio and R. A. Matzner, Phys. Rev. D **39**, 1046 (1989).

[35] H. Kurki-Suonio, R. A. Matzner, K. A. Olive, and D. N. Schramm, Astrophys. J. **353**, 406 (1990).

[36] H. Kurki-Suonio and R. A. Matzner, Phys. Rev. D **42**, 1047 (1990).

[37] D. N. Schramm and R. V. Wagoner, Annu. Rev. Nucl. Sci. **27**, 37 (1977).

[38] R. A. Malaney and W. A. Fowler, in *Origin and Distribution of the Elements,* proceedings of the Symposium, New Orleans, Louisiana, 1987, edited by G. J. Mathews (World Scientific, Singapore, 1988), p. 76.

[39] G. R. Caughlan, W. A. Fowler, M. J. Harris, and B. A. Zimmerman, At. Data Nucl. Data Tables **32**, 197 (1985).

[40] D. A. Dicus, E. W. Kolb, A. M. Gleeson, E. C. G. Sudarshan, V. L. Teplitz, and M. S. Turner, Phys. Rev. D **26**, 2694 (1982).

[41] W. H. Press and E. T. Vishniac, Astrophys. J. **239**, 1 (1980).

[42] S. Weinberg, *Gravitation and Cosmology* (Wiley, New York, 1972).